Eur. Phys. J. C 52, 83–92 (2007)
DOI 10.1140/epjc/s10052-007-0355-y

THE EUROPEAN PHYSICAL JOURNAL C

Regular Article – Theoretical Physics

Electroweak radiative corrections to the three channels of the process $f_1\bar{f}_1 HA \to 0$

D. Bardin[1], S. Bondarenko[2,a], L. Kalinovskaya[1], G. Nanava[3], L. Rumyantsev[1]

[1] Dzhelepov Laboratory for Nuclear Problems, JINR, Dubna, 141980, Russia
[2] Bogoliubov Laboratory of Theoretical Physics, JINR, Dubna, 141980, Russia
[3] IFJ, PAN, 31-342 Kraków, Poland

Received: 12 March 2007 / Revised version: 9 May 2007 /
Published online: 13 July 2007 –

Abstract. In this paper we describe the implementation of the complete next-to-leading order electroweak calculations for the various cross channels of the process $f_1\bar{f}_1 HA \to 0$ in the framework of the SANC system. Here A stands for a photon and f_1 for a fermion whose mass is neglected everywhere besides arguments of logarithmic functions. The symbol $\to 0$ means that all 4-momenta of the external particles flow inwards. The derived one-loop scalar form factors can be used for any cross channel after an appropriate permutation of their arguments s, t, u. We present the complete analytical results for the covariant and helicity amplitudes for three cross channels: $f_1\bar{f}_1 \to H\gamma$, $H \to f_1\bar{f}_1\gamma$ and $f_1\gamma \to f_1 H$. For checking of the correctness of the results first of all we observe the independence of the scalar form factors on the gauge parameters and the validity of the Ward identity (external photon transversality), and, secondly, we make an extensive comparison of our numerical results with other independent calculations.

PACS. 12.15.-y; 12.15.Lk

1 Introduction

Over the last twenty years, the standard model (SM) has provided an exceptionally accurate description of all high energy physics experiments. It is now tested at the 0.1% level. The only part of the SM that remains to be tested is the mechanism of electroweak symmetry breaking. In the SM, spontaneous symmetry breaking is achieved by the scalar Higgs field acquiring a vacuum expectation value, thereby giving mass to the quarks, leptons and gauge bosons. For an experimental investigation of the SM Higgs sector, it is necessary to fully understand and control higher order electroweak corrections to the processes involving the Higgs boson. In this paper we consider in detail a complete calculation of the full one-loop electroweak radiative corrections to the Higgs boson production processes $f_1\bar{f}_1 \to H\gamma$ and $e\gamma \to eH$, which could be observable at proposed muon colliders, given the expected integrated luminosities [1, 2], and at ILC [3]. Also we study the Higgs boson decay $H \to f_1\bar{f}_1\gamma$, which is interesting for physical applications at LHC [4].

Electroweak corrections to the Higgs production processes have been calculated before; see for example [5–10] (we quote only the papers with which we compare our numerical results). However, we were not able to find a paper in which the Higgs decay channel, $H \to f_1\bar{f}_1\gamma$, would be considered at next-to-leading order.

All the processes under consideration could be treated as the various cross channels of the process $f_1\bar{f}_1 H\gamma \to 0$, and hence one-loop corrected form factors (FM), derived for this process, can be used for its cross channels also, after an appropriate permutation of their arguments (s, t, u).

We pursue three goals: to demonstrate the analytic expressions for FFs at one-loop level (as an exception given their simplicity) and helicity amplitudes (HA) for three channels of the process $f_1\bar{f}_1 H\gamma \to 0$ (in the spirit of previous SANC presentations), and to compare the results with existing independent calculations. All results in this paper are obtained with the help of SANC (support of analytic and numerical calculations for experiments at colliders) – a network client–server system for semi-automatic calculations for various processes of elementary particle interactions at the one-loop precision level. The ideology of the calculation, precomputation modules, short user guide of the version V.1.00 and its installation are described in [11]. The SANC client may be downloaded from SANC servers [12, 13].

The paper is organized as follows. In Sect. 2 we demonstrate an analytic expression for the covariant amplitude (CA) at one-loop level in the annihilation channel and give explicit expressions for all FFs. Then we give HAs for all three channels available in SANC V.1.10. In Sect. 3 we show numerical results (computed by the s2n software)

[a] e-mail: bondarenko@jinr.ru

and comparison with the other independent calculations: for the decay channel $H \to f_1\bar{f}_1\gamma$ at tree level [14, 15], and in the resonance approximation at one-loop level [16]. For two channels $e^+e^- \to H\gamma$ and $e\gamma \to eH$ we compare with the one-loop level calculations of [5–7]. Finally, technical details related to the implementation of the considered processes into the SANC framework are collected in the appendix.

2 Amplitudes

We begin with a schematic representation of the diagram of the process $\bar{f}_1(p_1)f_1(p_2)\gamma(p_3)H(p_4) \to 0$ with all 4-momenta incoming, $p_1+p_2+p_3+p_4=0$. We will consider three cross channels of the process: annihilation, decay and H production. For all three channels we can write down an almost unique CA. Below we give it in the form corresponding to the annihilation channel, $\bar{f}(p_1)f(p_2) \to H(-p_4)\gamma(-p_3)$. It might easily be converted into any other channel by a proper permutation of external 4-momenta.

This is not the case, however, for the HA. The latter is different for all three channels and has to be calculated separately.

2.1 Covariant amplitude of the process

We have found that the CA of the process under study can be represented as a combination of eight structures transversal in photonic 4-momentum, four vector and four axial ones:

$$\begin{aligned}
\mathcal{A}_{\bar{f}_1 f_1 H\gamma} = \bar{v}\,(p_1) \Bigg\{ & \left[\frac{(p_2)_\nu}{T^2+m_f^2} - \frac{(p_1)_\nu}{U^2+m_f^2} \right. \\
& \left. + \frac{1}{2}\left(\frac{1}{T^2+m_f^2} + \frac{1}{U^2+m_f^2} \right) \not{p}_3 \gamma_\nu \right] \\
& \times F_{v1}\left(Q^2,T^2,U^2\right) \\
& + \left[\left(U^2+m_f^2\right)(p_2)_\nu - \left(T^2+m_f^2\right)(p_1)_\nu \right] \gamma_5 \\
& \times F_{a1}\left(Q^2,T^2,U^2\right) \\
& + \not{p}_3\gamma_\nu \left[F_{v2}\left(Q^2,T^2,U^2\right) + \gamma_5 F_{a2}\left(Q^2,T^2,U^2\right) \right] \\
& + \mathrm{i}\left[\not{p}_3 (p_1)_\nu - \frac{1}{2}\left(U^2+m_f^2\right)\gamma_\nu \right] \\
& \times \left[F_{v3}\left(Q^2,T^2,U^2\right) + \gamma_5 F_{a3}\left(Q^2,T^2,U^2\right) \right] \\
& + \mathrm{i}\left[\not{p}_3 (p_2)_\nu - \frac{1}{2}\left(T^2+m_f^2\right)\gamma_\nu \right] \\
& \times \left[F_{v4}\left(Q^2,T^2,U^2\right) + \gamma_5 F_{a4}\left(Q^2,T^2,U^2\right) \right] \Bigg\} \\
& \times u\,(p_2)\,\varepsilon_\nu^\gamma(p_3)\,, \qquad (1)
\end{aligned}$$

where $\bar{v}\,(p_1)$, $u\,(p_2)$ and m_f are the bispinors and the mass of the external fermions, respectively; $\varepsilon_\nu^\gamma(p_3)$ denotes the photon polarization vector. In (1) we intentionally keep the fermion mass in order to maintain photon transversality

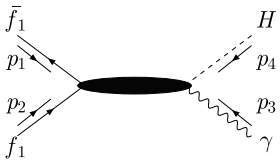

Fig. 1. The $\bar{f}_1 f_1 \gamma H \to 0$ process

without the mass approximation. Moreover in mass containing denominators in the first row the mass even cannot be neglected because they correspond to the fermionic propagators which emit an external photon, and thus lead to mass singularities.

All 4-momenta are incoming, and the usual Mandelstam invariants in Pauli metric ($p^2=-m^2$) are defined as follows:[1]

$$\begin{aligned}
&(p_1+p_2)^2 = Q^2 = -s, \quad (p_2+p_3)^2 = T^2 = -t, \\
&(p_2+p_4)^2 = U^2 = -u\,. \qquad (2)
\end{aligned}$$

Note that the representation (1) differs slightly from (53) of [11], as we found it appropriate to construct the Born-like amplitude as given in (58).

For the process of interest the CA at one-loop order has the form

$$\begin{aligned}
\mathcal{A}^{\text{Born + 1-loop}} = {} & \mathcal{A}^{\text{Born}}[\mathcal{O}(m_f)] + \mathcal{A}^{\text{1-loop}}[\mathcal{O}(\alpha)] \\
& + \mathcal{A}^{\text{1-loop}}[\mathcal{O}(m_f\alpha)]\,. \qquad (3)
\end{aligned}$$

Here the second term, $\mathcal{A}^{\text{1-loop}}[\mathcal{O}(\alpha)]$, stands for a part of the one-loop amplitude not suppressed by Yukawa coupling (m_f), contrary to the Born amplitude $\mathcal{A}^{\text{Born}}[\mathcal{O}(m_f)]$ and to the rest of the one-loop amplitude $\mathcal{A}^{\text{1-loop}}[\mathcal{O}(m_f\alpha)]$. For this reason the Born amplitude typically contributes less than the one-loop one. Since the f cannot be a top quark, for all channels one may neglect the third term. Then for the squared amplitude one has

$$|\mathcal{A}^{\text{Born + 1-loop}}|^2 \longrightarrow |\mathcal{A}^{\text{Born}}[\mathcal{O}(m_f)] + \mathcal{A}^{\text{1-loop}}[\mathcal{O}(\alpha)]|^2\,. \qquad (4)$$

For the first generation fermions even $\mathcal{A}^{\text{Born}}$ should be neglected, but it can be significant for the second and third generations. Note that the QED one-loop and the bremsstrahlung corrections contribute to the third term of (3), so they could safely be neglected.

2.2 Diagrams contributing to $\mathcal{A}^{\text{1-loop}}[\mathcal{O}(\alpha)]$, form factors

Here we discuss which one-loop Feynman diagrams contribute to $\mathcal{A}^{\text{1-loop}}[\mathcal{O}(\alpha)]$, not suppressed by a Yukawa coupling. For definiteness, we discuss the annihilation channel. There are only a few of them.

1. First, we have the "right" three-boson ($B\gamma H$, $B=\gamma, Z$) vertex; see Fig. 6 of [17]. The diagram with $B=\gamma$ leads

[1] In this section we will use the notation Q^2, T^2, U^2, emphasizing thereby that we do not fix the channel yet.

to a Coulomb singularity for the decay and production channels.
2. Next, we have boxes of the T1 and T3 topologies with a virtual W boson; see Fig. 15 of [11].
3. Then we have a box of the T5 topology with a virtual Z boson; see Fig. 16a of [11].
4. Also, there are associated WW and ZZ vertices of the topology BFB; see Fig. 10b of [11].

As was motivated above, in general, we keep the two Born diagrams of the kind shown in Fig. 1 of [17].

Every FF is presented as the sum over the gauge index ($1 = \xi_A, 2 = \xi_Z, 3 = \xi_W \equiv \xi, 4 = \text{without } \xi$):

$$F_{v(a)i}(Q^2,T^2,U^2) = \sum_{k=1,4} F_{v(a)ik}(Q^2,T^2,U^2)\,. \quad (5)$$

Obviously, $k = 1$ does not contribute in the massless case. The FF for $k = 2, 3, 4$ are rather compact; they are shown in the next section.

2.3 One-loop form factors

The complete analytic results for the FF were presented in the literature earlier; see e.g. [7] and references therein. The aim of the presentation of this section is to show a typical SANC result for the FF in terms of only *scalar* Passarino–Veltman (PV) functions of [18].[2]

In the limit $m_f \to 0$ the FF with the gauge index 2 take a simple form:

$$\begin{aligned}
F_{v32}(Q^2,T^2,U^2) &= Q_f \frac{v_f^2+a_f^2}{2} F_2(Q^2,T^2,U^2)\,,\\
F_{v42}(Q^2,T^2,U^2) &= Q_f \frac{v_f^2+a_f^2}{2} F_2(Q^2,U^2,T^2)\,,\\
F_{a32}(Q^2,T^2,U^2) &= Q_f v_f a_f F_2(Q^2,T^2,U^2)\,,\\
F_{a42}(Q^2,T^2,U^2) &= Q_f v_f a_f F_2(Q^2,U^2,T^2)\,, \quad (6)
\end{aligned}$$

where an auxiliary function was introduced:

$$\begin{aligned}
&F_2\left(Q^2,T^2,U^2\right)\\
&= \frac{s_{\rm W}}{c_{\rm W}^3}\frac{M_Z}{Q^2U^2}\left\{\left(M_Z^2+U^2\right)\frac{1}{U^2}\right.\\
&\times C_{d_0c_0}\left(T^2,U^2,-M_H^2;M_Z\right) + \left(M_Z^2+U^2\right)\left(M_H^2+U^2\right)\\
&\times \frac{1}{U^2} C_0\left(-M_H^2,-m_f^2,U^2;M_Z,M_Z,m_f\right)\\
&+ \left[Q^2-U^2+M_Z^2\left(1+\frac{Q^2}{U^2}+2\frac{U^2}{T^2+M_H^2}\right)\right]\\
&\times C_0\left(-M_H^2,-m_f^2,T^2;M_Z,M_Z,m_f\right) - \frac{2Q^2}{T^2+M_H^2}\\
&\left.\times\left[B_0^F\left(-M_H^2;M_Z,M_Z\right) - B_0^F\left(T^2;M_Z,m_f\right)\right]\right\}. \quad (7)
\end{aligned}$$

[2] We do it only once in this paper, by way of exception; usually we refer the reader to the equations generated by FF modules of the system itself.

Here $C_{d_0c_0}$ stands for a particular combination of PV functions that is explicitly free of fermionic mass singularities, contrary to individual terms which are not (this is why one must keep the masses in the arguments of mass singular PV functions). It has the form

$$\begin{aligned}
&C_{d_0c_0}(T^2,U^2,-M_H^2;M_Z)\\
&= \left[-T^2U^2-\left(T^2+U^2\right)M_Z^2\right]\\
&\quad\times D_0(0,-m_f^2,-M_H^2,-m_f^2,T^2,U^2;m_f,m_f,M_Z,M_Z)\\
&\quad + T^2 C_0(0,-m_f^2,T^2;m_f,m_f,M_Z)\\
&\quad + U^2 C_0(0,-m_f^2,U^2;m_f,m_f,M_Z)\,. \quad (8)
\end{aligned}$$

The FF with gauge index 4 are

$$\begin{aligned}
F_{v34}(Q^2) &= F_{v44}(Q^2)\\
&= 2\sum_i s_{\rm W} c_i \frac{m_i^2}{M_{\rm W}}\\
&\quad\times\left(4\frac{Q_f Q_i^2 s_{\rm W}^2}{Q^2} + \frac{v_f Q_i v_i}{c_{\rm W}^2}\frac{1}{Q^2+M_Z^2}\right)F_{4i}(Q^2)\,,\\
F_{a34}(Q^2) &= F_{a44}(Q^2)\\
&= 2\sum_i s_{\rm W} c_i \frac{m_i^2}{M_{\rm W}}\left(\frac{a_f Q_i v_i}{c_{\rm W}^2}\frac{1}{Q^2+M_Z^2}\right)F_{4i}(Q^2)\,,
\end{aligned} \quad (9)$$

with the index i running over fermion families, and the auxiliary function reads

$$\begin{aligned}
F_{4i}(Q^2) &= \left(\frac{1}{2}-\frac{2m_i^2}{Q^2+M_H^2}\right)C_0(0,-M_H^2,Q^2,m_i,m_i,m_i)\\
&\quad + \frac{1}{Q^2+M_H^2}\left[1-\frac{Q^2}{Q^2+M_H^2}\left(B_0^F\left(-M_H^2;m_i,m_i\right)\right.\right.\\
&\quad \left.\left. - B_0^F\left(Q^2;m_i,m_i\right)\right)\right]. \quad (10)
\end{aligned}$$

The FF with gauge index 3 are more cumbersome:

$$\begin{aligned}
F_{v33}(Q^2,T^2,U^2) &= Q_f F_{q3}(Q^2) + v_f F_{va3}(Q^2)\\
&\quad + F_3(Q^2,T^2,U^2)\,,\\
F_{v43}(Q^2,T^2,U^2) &= Q_f F_{q3}(Q^2) + v_f F_{va3}(Q^2)\\
&\quad + F_3(Q^2,U^2,T^2)\,,\\
F_{a33}(Q^2,T^2,U^2) &= a_f F_{va3}(Q^2) + F_3(Q^2,T^2,U^2)\,,\\
F_{a43}(Q^2,T^2,U^2) &= a_f F_{va3}(Q^2) + F_3(Q^2,U^2,T^2)\,,
\end{aligned} \quad (11)$$

and one needs three auxiliary functions to define them:

$$\begin{aligned}
F_{q3}(Q^2) &= 2\frac{s_{\rm W}^3}{M_{\rm W}}\left\{-2\frac{M_{\rm W}^2}{Q^2}\left(4-\frac{M_H^2+6M_{\rm W}^2}{Q^2+M_H^2}\right)\right.\\
&\quad\times C_0(0,-M_H^2,Q^2;M_{\rm W},M_{\rm W},M_{\rm W}) + \frac{M_H^2+6M_{\rm W}^2}{Q^2+M_H^2}\\
&\quad\left[\frac{1}{Q^2+M_H^2}\left(B_0^F\left(-M_H^2;M_{\rm W},M_{\rm W}\right)\right.\right.\\
&\quad\left.\left.\left. - B_0^F\left(Q^2;M_{\rm W},M_{\rm W}\right)\right) - \frac{1}{Q^2}\right]\right\},
\end{aligned}$$

$$
\begin{aligned}
F_{va3}(Q^2) = \frac{s_{\rm W}}{M_{\rm W}}\Bigg\{ & \frac{1}{Q^2+M_Z^2}\Bigg[\left(\frac{1}{c_{\rm W}^2}-6-\left(\frac{1}{c_{\rm W}^2}-12c_{\rm W}^2\right)\right.\\
& \left.\times\frac{M_Z^2}{Q^2+M_H^2}\right)M_{\rm W}^2 C_0(0,-M_H^2,Q^2;M_{\rm W},M_{\rm W},M_{\rm W})\\
& +\left(\frac{1}{2c_{\rm W}^2}-1+\left(\frac{1}{2c_{\rm W}^2}-6c_{\rm W}^2\right)\frac{M_Z^2}{Q^2+M_H^2}\right)\\
& \times\left(\frac{M_Z^2}{Q^2+M_H^2}\left(B_0^F\left(-M_H^2;M_{\rm W},M_{\rm W}\right)\right.\right.\\
& \left.\left.-B_0^F\left(Q^2;M_{\rm W},M_{\rm W}\right)\right)+1\right)\Bigg]+\frac{1}{Q^2+M_H^2}\Bigg[\left(\frac{1}{c_{\rm W}^2}-2\right)\\
& \times M_{\rm W}^2 C_0(0,-M_H^2,Q^2;M_{\rm W},M_{\rm W},M_{\rm W})\\
& +\frac{M_Z^2}{Q^2+M_H^2}\left(-\frac{1}{2c_{\rm W}^2}+6c_{\rm W}^2+\left(1-\frac{1}{2c_{\rm W}^2}\right)\frac{M_H^2}{M_Z^2}\right)\\
& \times\left(B_0^F\left(-M_H^2;M_{\rm W},M_{\rm W}\right)-B_0^F\left(Q^2;M_{\rm W},M_{\rm W}\right)\right)\\
& -\frac{1}{2c_{\rm W}^2}+1\Bigg]\Bigg\},\\
F_3(Q^2,T^2,U^2) = \frac{1}{2}s_{\rm W}M_{\rm W}\Bigg\{ & \frac{1}{Q^2U^4}\left[\left(U^2+M_{\rm W}^2\right)\right.\\
& \times\left(Q^2\left(U^2+M_{\rm W}^2\right)+M_{\rm W}^2M_H^2\right)\,d_{0\rm aux}(Q^2,U^2)\\
& +\left(\left[\left(U^2+M_{\rm W}^2\right)M_{\rm W}^2+Q^2T^2\right]M_H^2+2Q^2U^2M_{\rm W}^2\right.\\
& \left.+Q^2\left(T^2-M_{\rm W}^2\right)^2\right)\,d_{0\rm aux}(Q^2,T^2)\\
& +Q^4C_0\left(-m_f^2,-m_f^2,Q^2;M_{\rm W},0,M_{\rm W}\right)+\left(Q^2+M_H^2\right)\\
& \times\left[Q^2+2\left(U^2+M_{\rm W}^2\right)\right]C_0\left(0,-M_H^2,Q^2;M_{\rm W},M_{\rm W},M_{\rm W}\right)\\
& +\left(Q^2\left(T^2+M_H^2\right)+\left(U^2+M_{\rm W}^2\right)(U^2-Q^2)\right.\\
& \left.+2\frac{M_{\rm W}^2Q^2U^2}{T^2+M_H^2}\right)C_0\left(-M_H^2,-m_f^2,T^2;M_{\rm W},M_{\rm W},0\right)\\
& -\left(U^2+M_H^2\right)\left(U^2+M_{\rm W}^2\right)\\
& \times C_0\left(-M_H^2,-m_f^2,U^2;M_{\rm W},M_{\rm W},0\right)\\
& +T^2\left(Q^2+U^2+M_{\rm W}^2\right)C_0\left(0,-m_f^2,T^2;M_{\rm W},M_{\rm W},0\right)\\
& \left.+U^2\left(U^2+M_{\rm W}^2\right)C_0\left(0,-m_f^2,U^2;M_{\rm W},M_{\rm W},0\right)\right]\\
& +\frac{2}{U^2}\frac{1}{T^2+M_H^2}\left(B_0^F\left(-M_H^2;M_{\rm W},M_{\rm W}\right)\right.\\
& \left.-B_0^F\left(T^2;M_{\rm W},0\right)\right)\Bigg\}\,. \qquad (12)
\end{aligned}
$$

Here two more short hand notations are introduced:

$$
\begin{aligned}
& d_{0\rm aux}(Q^2,T^2)\\
& = D_0(-m_f^2,-m_f^2,0,-M_H^2,Q^2,T^2;M_{\rm W},0,M_{\rm W},M_{\rm W})\,,\\
& d_{0\rm aux}(Q^2,U^2)\\
& = D_0(-m_f^2,-m_f^2,-M_H^2,0,Q^2,U^2;M_{\rm W},0,M_{\rm W},M_{\rm W})\,.
\end{aligned} \qquad (13)
$$

2.4 Helicity amplitudes

In this section we collect the analytical expressions of the HAs for all three channels.

2.4.1 Annihilation channel $\bar{f}_1 f_1 \to H\gamma$

We begin by considering HA for the annihilation process

$$
\bar{f}_1(p_1,\lambda_1)+f_1(p_2,\lambda_2)\to\gamma(p_3,\lambda_3)+H(p_4)\,, \qquad (14)
$$

$\lambda_i (i=1,2,3)$ being the helicities of the external particles. The CA for this channel can be obtained from (1) with the following permutation of the 4-momenta:

$$
\begin{aligned}
& p_1\to p_1,\\
& p_2\to p_2,\\
& p_3\to -p_3,\\
& p_4\to -p_4\,.
\end{aligned}
$$

The set of corresponding HA, which we denote as $\mathcal{H}_{\lambda_1\lambda_2\lambda_3}$, for this case reads[3]

$$
\begin{aligned}
\mathcal{H}_{\pm\pm\pm} = & \mp k_0\left[\frac{-Z_4(M_H)\beta_+/2+s\beta^2}{Z_1(m_f)Z_2(m_f)}F_{v1}(s,t)\right.\\
& \mp s\beta F_{a1}(s,t)-\beta_+\left(F_{v2}(s,t)\mp F_{a2}(s,t)\right)\\
& +m_f\left(F_{v3}(s,t)\mp\beta F_{a3}(s,t)\right)\\
& \left.+m_f\left(F_{v4}(s,t)\pm\beta F_{a4}(s,t)\right)\right],\\
\mathcal{H}_{\pm\pm\mp} = & \pm k_0\left[\frac{-Z_4(M_H)\beta_-/2+s\beta^2}{Z_1(m_f)Z_2(m_f)}F_{v1}(s,t)\right.\\
& \mp s\beta F_{a1}(s,t)-\beta_-\left(F_{v2}(s,t)\pm F_{a2}(s,t)\right)\\
& +m_f\left(F_{v3}(s,t)\mp\beta F_{a3}(s,t)\right)\\
& \left.+m_f\left(F_{v4}(s,t)\pm\beta F_{a4}(s,t)\right)\right],\\
\mathcal{H}_{\pm\mp\pm} = & -k_+\left[\frac{2m_f}{s}\frac{Z_4(M_H)}{Z_1(m_f)Z_2(m_f)}F_{v1}(s,t)\right.\\
& +\frac{4m_f}{s}\left(F_{v2}(s,t)\mp F_{a2}(s,t)\right)\\
& -\beta_+\left(F_{v3}(s,t)\pm\beta F_{a3}(s,t)\right)\\
& \left.-\beta_-\left(F_{v4}(s,t)\pm\beta F_{a4}(s,t)\right)\right],\\
\mathcal{H}_{\pm\mp\mp} = & -k_-\left[\frac{2m_f}{s}\frac{Z_4(M_H)}{Z_1(m_f)Z_2(m_f)}F_{v1}(s,t)\right.\\
& +\frac{4m_f}{s}\left(F_{v2}(s,t)\pm F_{a2}(s,t)\right)\\
& -\beta_-\left(F_{v3}(s,t)\pm\beta F_{a3}(s,t)\right)\\
& \left.-\beta_+\left(F_{v4}(s,t)\pm\beta F_{a4}(s,t)\right)\right]\,, \qquad (15)
\end{aligned}
$$

where the coefficients

$$
\begin{aligned}
k_0 &= \sin\vartheta_\gamma\frac{s-M_H^2}{2\sqrt{2}}\,,\\
k_\pm &= c_\pm\frac{(s-M_H^2)\sqrt{s}}{4\sqrt{2}}\,,
\end{aligned} \qquad (16)
$$

[3] In the argument list of FF, e.g. $F_{v1}(s,t)$, we drop the "$-$" signs, which appear due to the convention of (2) and the non-independent invariant u. This is done only for the sake of readability; both the "$-$" signs and u are explicitly present in our FORTRAN codes.

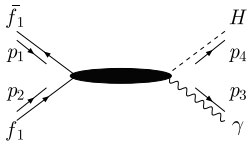

Fig. 2. Schematic representation of one-loop Feynman diagrams for the annihilation channel

with

$$c_\pm = 1 \pm \cos\vartheta_\gamma\,, \quad \beta_\pm = 1 \pm \beta\,,$$
$$\beta = \sqrt{\lambda\left(s, m_f^2, m_f^2\right)}/s\,, \tag{17}$$

and the fermionic propagators and t, u invariants are

$$Z_1(m_f) = \frac{1}{2} Z_4(M_H)\,(1 + \beta\cos\vartheta_\gamma)\,,$$
$$Z_2(m_f) = \frac{1}{2} Z_4(M_H)\,(1 - \beta\cos\vartheta_\gamma)\,,$$
$$t = m_f^2 - Z_2(m_f), \quad u = m_f^2 - Z_1(m_f)\,. \tag{18}$$

Here $Z_4(M_H) = s - M_H^2$, and ϑ_γ is the angle of the produced photon (angle between momenta $\mathbf{p}_2$ and $\mathbf{p}_3$) in the center of mass system.

2.4.2 Decay channel $H \to f_1\bar{f}_1\gamma$

In this section we consider the HA for the Higgs boson decay channel

$$H(p_2) \to \gamma(p_1, \lambda_1) + f_1(p_3, \lambda_3) + \bar{f}_1(p_4, \lambda_4)\,, \tag{19}$$

where $\lambda_i (i = 1, 3, 4)$ are the helicities of the external particles.

In order to obtain the CA for this channel the 4-momenta permutations in (1) are chosen as follows:

$$p_1 \to -p_3,$$
$$p_2 \to -p_4,$$
$$p_3 \to -p_1,$$
$$p_4 \to p_2\,.$$

The HA, which we denote as $\mathcal{H}_{\lambda_1\lambda_3\lambda_4}$, for this channel are somewhat similar to the annihilation ones:

$$\begin{aligned}
\mathcal{H}_{\pm\pm\pm} = k_0 \Bigg[& \frac{\beta_- Z_2(M_H)/2 + s\beta^2}{Z_3(m_f) Z_4(m_f)} F_{v1}(s,t) \\
& \pm \beta s F_{a1}(s,t) - \beta_- \left(F_{v2}(s,t) \mp F_{a2}(s,t)\right) \\
& + m_f \left(F_{v3}(s,t) \pm \beta F_{a3}(s,t)\right) \\
& + m_f \left(F_{v4}(s,t) \mp \beta F_{a4}(s,t)\right)\Bigg]\,, \\
\mathcal{H}_{\pm\mp\mp} = k_0 \Bigg[& \frac{\beta_+ Z_2(M_H)/2 + s\beta^2}{Z_3(m_f) Z_4(m_f)} F_{v1}(s,t) \\
& \mp \beta s F_{a1}(s,t) - \beta_+ \left(F_{v2}(s,t) \mp F_{a2}(s,t)\right) \\
& + m_f \left(F_{v3}(s,t) \mp \beta F_{a3}(s,t)\right) \\
& + m_f \left(F_{v4}(s,t) \pm \beta F_{a4}(s,t)\right)\Bigg]\,,
\end{aligned}$$

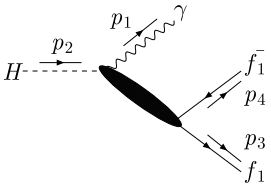

Fig. 3. Schematic representation of one-loop Feynman diagram for the decay channel

$$\begin{aligned}
\mathcal{H}_{\pm\mp\pm} = k_+ \Bigg[& \mp \frac{2m_f}{s} \frac{Z_2(M_H)}{Z_3(m_f) Z_4(m_f)} F_{v1}(s,t) \\
& \pm \frac{4m_f}{s} \left(F_{v2}(s,t) \mp F_{a2}(s,t)\right) \\
& \mp \beta_+ \left(F_{v3}(s,t) \pm \beta F_{a3}(s,t)\right) \\
& \mp \beta_- \left(F_{v4}(s,t) \pm \beta F_{a4}(s,t)\right)\Bigg]\,, \\
\mathcal{H}_{\pm\pm\mp} = k_- \Bigg[& \mp \frac{2m_f}{s} \frac{Z_2(M_H)}{Z_3(m_f) Z_4(m_f)} F_{v1}(s,t) \\
& \pm \frac{4m_f}{s} \left(F_{v2}(s,t) \mp F_{a2}(s,t)\right) \\
& \mp \beta_- \left(F_{v3}(s,t) \mp \beta F_{a3}(s,t)\right) \\
& \mp \beta_+ \left(F_{v4}(s,t) \mp \beta F_{a4}(s,t)\right)\Bigg]\,,
\end{aligned} \tag{20}$$

where the coefficients are

$$k_0 = \frac{M_H^2 - s}{2\sqrt{2}} \sin\vartheta_f\,,$$
$$k_\pm = c_\pm \frac{\left(M_H^2 - s\right)\sqrt{s}}{4\sqrt{2}}\,,$$
$$c_\pm = 1 \pm \cos\vartheta_f\,, \tag{21}$$

and the fermionic propagators and s, t, u invariants are

$$Z_3(m_f) = \frac{1}{2} Z_2(M_H)\,(1 + \beta\cos\vartheta_f)\,,$$
$$Z_4(m_f) = \frac{1}{2} Z_2(M_H)\,(1 - \beta\cos\vartheta_f)\,,$$
$$s = M_{f\bar{f}}^2, \quad t = m_f^2 + Z_4(m_f), \quad u = m_f^2 + Z_3(m_f)\,, \tag{22}$$

with $Z_2(M_H) = M_H^2 - s$ and ϑ_f being the angle between the vector $\mathbf{p}_4$ and the direction defined by the photon momentum $\mathbf{p}_1$, which is chosen to be the direction of the z-axes of the $(\mathbf{p}_3, \mathbf{p}_4)$ rest frame.

2.4.3 H production channel $e\gamma \to eH$

For this channel we present the HA for two cases: for the limit $m_e \to 0$ and for the case exact in m_e.

The CA for the H production channel,

$$\gamma(p_1, \lambda_1) + e(p_2, \lambda_2) \to e(p_3, \lambda_3) + H(p_4)\,, \tag{23}$$

are obtained from (1) with the help of the permutations

$$p_1 \to -p_3,$$
$$p_2 \to p_2,$$
$$p_3 \to p_1,$$
$$p_4 \to -p_4\,.$$

The HA, denoted as $\mathcal{H}_{\lambda_1\lambda_2\lambda_3}$ (λ_i $(i=1,2,3)$ being the helicities of the external particles), in the small mass limit are remarkably compact:

$$\begin{aligned}
\mathcal{H}_{\pm\pm\pm} &= \pm k_1 \left[F_{v4}(s,t) \mp F_{a4}(s,t)\right], \\
\mathcal{H}_{\mp\pm\pm} &= \mp k_2 \left[F_{v3}(s,t) \mp F_{a3}(s,t)\right], \\
\mathcal{H}_{\mp\mp\pm} &= k_3 \Bigg[\frac{M_H^2}{Z_3(m_e)} F_{v1}(s,t) \pm k F_{a1}(s,t) \\
&\quad + 2s\left(F_{v2}(s,t) \pm F_{a2}(s,t)\right)\Bigg], \\
\mathcal{H}_{\mp\pm\mp} &= k_3 \left[\left(\frac{s_h}{Z_3(m_e)} - 1\right) F_{v1}(s,t) \pm k F_{a1}(s,t)\right],
\end{aligned} \tag{24}$$

with the coefficients:

$$\begin{aligned}
k &= c_- \frac{s s_h}{2}, \quad k_1 = s\sqrt{\frac{s_h}{2}} \sin\frac{\vartheta_f}{2}, \\
k_2 &= c_+ \frac{(s_h)^{3/2}}{2\sqrt{2}} \sin\frac{\vartheta_f}{2}, \quad k_3 = \sqrt{\frac{s_h}{2s}} \cos\frac{\vartheta_f}{2}, \\
s_h &= s - M_H^2 .
\end{aligned} \tag{25}$$

The fermionic propagators exact in m_e are

$$\begin{aligned}
Z_2(m_e) &= s - m_e^2 , \\
Z_3(m_e) &= \frac{Z_2(m_e)}{2s} \\
&\quad \times \left[s + m_e^2 - M_H^2 + \sqrt{\lambda(s, m_e^2, M_H^2)} \cos\vartheta_f\right].
\end{aligned} \tag{26}$$

The Mandelstam variables transform as follows:

$$\begin{aligned}
s &\to -\frac{1}{2}\left[\left(s - \frac{M_H^2 m_e^2}{s} - M_H^2 - 2m_e^2 + \frac{m_e^4}{s}\right)\right. \\
&\quad \left. - \frac{s - m_e^2}{s}\sqrt{\lambda(s, m_e^2, M_H^2)} \cos\vartheta_f\right], \\
t &\to s, \\
u &\to -\frac{1}{2}\left[\left(s + \frac{M_H^2 m_e^2}{s} - M_H^2 - 2m_e^2 - \frac{m_e^4}{s}\right)\right. \\
&\quad \left. + \frac{s - m_e^2}{s}\sqrt{\lambda(s, m_e^2, M_H^2)} \cos\vartheta_f\right].
\end{aligned} \tag{27}$$

For $Z_2(m_e)$ here we use massless expressions, while for $Z_3(m_e)$ we use the exact one, since it develops a logarithmic mass singularity. For the massive case below, we use all expressions exact in the masses. Also important quantities for this channel are

$$\begin{aligned}
N_\pm^2 &= \frac{1}{4}\left(s + 6m_e^2 - M_H^2 + \frac{m_e^2(m_e^2 - M_H^2)}{s}\right. \\
&\quad \left. \mp \frac{s - m_e^2}{s}\sqrt{\lambda(s, m_e^2, M_H^2)}\right).
\end{aligned} \tag{28}$$

In the massless case only N_- contributes, and its limit is

$$N_- = \sqrt{\frac{s_h}{2}} . \tag{29}$$

The fully massive case has the following form:

$$\begin{aligned}
&\mathcal{H}_{\pm\pm\pm} \\
&= \sin\frac{\vartheta_f}{2}\left[\pm\frac{1}{Z_2(m_e)Z_3(m_e)}\right. \\
&\quad \times \left(\sqrt{s}\left[M_H^2 - m_e^2(4 + r_{d_2}\cos\vartheta_f)\right] N_+\right. \\
&\quad + \frac{m_e}{2}\left(3s_h + m_e^2(9 - r_{d_1})\right. \\
&\quad \left.\left. + \left[s_h + m_e^2(3 + r_{d_1})\right]\cos\vartheta_f\right) N_-\right) F_{v1}(s,t) \\
&\quad - s_m c_+ \left[\frac{\sqrt{s}}{2}(-2 + r_{d_1})N_+ - m_e N_-\right] F_{a1}(s,t) \\
&\quad \pm 2\left(\sqrt{s}N_+ - m_e N_-\right)\left(F_{v2}(s,t) \mp F_{a2}(s,t)\right) \\
&\quad \mp \frac{m_e}{2}\left[\sqrt{s}\left(4 - r_{d_1} + r_{d_3}\cos\vartheta_f\right) N_+\right. \\
&\quad \left. - m_e\left(4 - r_{d_1} c_-\right) N_-\right] F_{v3}(s,t) \\
&\quad + \frac{m_e}{2}\left[\sqrt{s}\left(r_{d_1} - r_{d_3}\cos\vartheta_f\right) N_+ - m_e r_{d_1} c_- N_-\right] \\
&\quad \times F_{a3}(s,t) \\
&\quad \mp \left[2\sqrt{s} m_e N_+ - (s + m_e^2) N_-\right] F_{v4}(s,t) \\
&\quad \left. - s_m N_- F_{a4}(s,t)\right], \\
&\mathcal{H}_{\mp\pm\pm} \\
&= \sin\frac{\vartheta_f}{2} c_+ \left[\pm\frac{1}{Z_2(m_e)Z_3(m_e)}\right. \\
&\quad \left(\frac{\sqrt{s}}{2}\left[s_h + m_e^2(3 + r_{d_1})\right] N_+ - s m_e r_{d_2} N_-\right) F_{v1}(s,t) \\
&\quad + \left(\frac{\sqrt{s}}{2}\left[s_h + m_e^2(3 - r_{d_1})\right] N_+ - s_m m_e N_-\right) F_{a1}(s,t) \\
&\quad \left. \pm \frac{1}{2}\left(\sqrt{s} m_e r_{d_1} N_+ - s r_{d_3} N_-\right)\left(F_{v3}(s,t) \mp F_{a3}(s,t)\right)\right], \\
&\mathcal{H}_{\mp\mp\pm} \\
&= \cos\frac{\vartheta_f}{2}\left[\frac{1}{Z_2(m_e)Z_3(m_e)}\right. \\
&\quad \left(\frac{m_e}{2}\left(3s_h + m_e^2(9 - r_{d_1})\right.\right. \\
&\quad \left. - \left[s_h + m_e^2(3 + r_{d_1})\right]\cos\vartheta_f\right) N_+ \\
&\quad \left. + \sqrt{s}\left[M_H^2 - m_e^2(4 - r_{d_2}\cos\vartheta_f)\right] N_-\right) F_{v1}(s,t) \\
&\quad \mp c_- \left(s_m m_e N_+ - \frac{\sqrt{s}}{2}\left[s_h + m_e^2(3 - r_{d_1})\right] N_-\right) \\
&\quad \times F_{a1}(s,t)
\end{aligned}$$

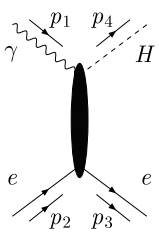

Fig. 4. Schematic representation of one-loop Feynman diagrams for $e\gamma \to eH$ channel

$$
\begin{aligned}
&-2\left(m_e N_+ - \sqrt{s}N_-\right)\left(F_{v2}(s,t) \pm F_{a2}(s,t)\right)\\
&+\frac{m_e}{2}\Big[m_e\left(4-r_{d_1}c_+\right)N_+ - \sqrt{s}\left(4-r_{d_1}-r_{d_3}\cos\vartheta_f\right)\\
&\times N_-\Big]F_{v3}(s,t) \pm \frac{m_e}{2}\\
&\times\Big[m_e r_{d_1}c_+ N_+ - \sqrt{s}\left(r_{d_1}+r_{d_3}\cos\vartheta_f\right)N_-\Big]F_{a3}(s,t)\\
&+\left[(s+m_e^2)N_+ - 2\sqrt{s}m_e N_-\right]F_{v4}(s,t)\\
&\pm s_m N_+ F_{a4}(s,t)\Big],\\
\mathcal{H}_{\mp\pm\mp}&\\
&=\cos\frac{\vartheta_f}{2}c_-\left[\frac{1}{Z_2(m_e)Z_3(m_e)}\right.\\
&\left(-sm_e r_{d_2}N_+ + \frac{\sqrt{s}}{2}\left[s_h + m_e^2(3+r_{d_1})\right]N_-\right)F_{v1}(s,t)\\
&\mp\left(s_m m_e N_+ - \frac{\sqrt{s}}{2}\left[s_h + m_e^2(3-r_{d_1})\right]N_-\right)F_{a1}(s,t)\\
&\left.-\frac{1}{2}\left(sr_{d_3}N_+ - \sqrt{s}m_e r_{d_1}N_-\right)\left(F_{v3}(s,t)\mp F_{a3}(s,t)\right)\right],
\end{aligned}
\tag{30}
$$

where

$$
\begin{aligned}
&s_m = s - m_e^2, \quad r_{d_1} = 3 - \frac{M_H^2 - m_e^2}{s},\\
&r_{d_2} = 2 - \frac{M_H^2 - 2m_e^2}{s}, \quad r_{d_3} = 1 - \frac{M_H^2 - 3m_e^2}{s}
\end{aligned}
\tag{31}
$$

and ϑ_f is the cms angle of the final fermion (angle between momenta $\mathbf{p}_2$ and $\mathbf{p}_3$).

3 Numerical results and comparison

In this section we present results of numerical calculations and comparisons with other groups.

3.1 Annihilation channel $f_1\bar{f}_1 \to \gamma H$

There are many papers that are devoted to this channel; see for example [5–7] and references therein. It is highly non-trivial to realize a tuned comparison of the numerical results, since the authors do not present the list of input parameters and do not specify the calculational scheme, although stating agreement among themselves. Eventually, we found it best to compare with the most recent paper [7], namely with Fig. 2, showing the M_H dependence of the total cross section for the two values of $\sqrt{s} = 500$ (solid line) and 1500 GeV (dashed line). As can be judged from a comparison of their figures with ours, there is qualitative agreement of the cross sections. One should emphasize that we did not find in [7] which value of the top quark mass is used on which we observed quite a strong dependence. For example, at $\sqrt{s} = 500$ GeV and $M_H = 300$ GeV, the cross section equals 1.32×10^{-2} fb for $m_t = 174.2$ GeV and 1.89×10^{-2} fb for $m_t = 140$ GeV.

Note that all the numerical results of this section are produced with the so-called Standard SANC INPUT (Sect. 6.2.3 of [17]).

3.2 Decay channel $H \to f_1\bar{f}_1\gamma$

For the decay channel we did not find in the literature complete one-loop calculations. We present here numerical results for the $H \to \mu^+\mu^-\gamma$ decay channel for $M_H = 150$ GeV.

- First we consider GRACE, CompHEP and SANC at the Born level.
  The results of the comparison for the total width in the Born approximation between GRACE [15], CompHEP [14] and SANC are shown in Table 1. Here the input parameters are as in CompHEP.
  Note that SANC produces stable results up to very small photon energies, which is mandatory to have correct matching of soft and hard radiations.
- Next we consider SANC at the Born and one-loop levels.
  In Fig. 6 the fermion–antifermion invariant mass distribution, $\mathrm{d}\Gamma/\mathrm{d}M_{\mu^+\mu^-}$ is demonstrated.
  Two peaks due to γ and Z exchanges are distinctly seen. The Coulomb peak region usually does not represent anything of interest and should be cut out.
  In Table 2, the partial width is shown in dependence on the cut values of the lower and upper limits of invariant mass of the $\mu^+\mu^-$ pair, $s_{q\min}$ and $s_{q\max}$, $(s_q = M_{\mu^+\mu^-})$, in the Born and one-loop approximation in two the schemes α and G_F.
  All parameters and numbers are in GeV. The two first $s_{q\max}$ are calculated in terms of E_γ cut by the equation $s_{q\max}^2 = M_H^2 - 2M_H E_\gamma$ for $E_\gamma = 1$ and 10 GeV, respectively. As can be seen, the major part of the one-loop decay width is due to a Z resonance.
- Now we look at SANC in the resonance approximation at one-loop level.
  The latter observation justifies to a certain extent the usual approach to the calculation of this decay, the one-

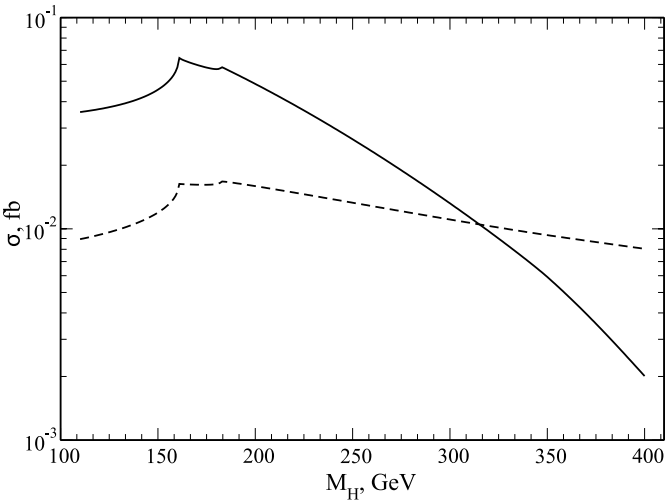

Fig. 5. One-loop corrected cross section of the Higgs boson production via annihilation process, as a function of the Higgs boson mass, M_H. The *solid* and *dashed lines* correspond to the results evaluated respectivaly at $\sqrt{s} = 500$ and $\sqrt{s} = 1500$

loop resonance approximation, which is realized for example in PYTHIA [16]:

$$\Gamma^{\text{Res 1-loop}}_{H\to\mu^+\mu^-\gamma} = \frac{\Gamma^{\text{1-loop}}_{H\to Z\gamma}\Gamma^{\text{1-loop}}_{Z\to\mu^+\mu^-}}{\Gamma_Z}\,. \qquad (32)$$

In Table 3, the total width is shown in dependence on the cut value, $s_{q\min}$, in the resonance one-loop and in the complete one-loop approximations, again in the α and $G_{\rm F}$ schemes. Here, however, this is done without the Born amplitude which is why only one cut from below is applied.

Comparing columns computed in the same schemes, we see that the resonance approximation works with 2% percent accuracy for the strong cuts (50,70) GeV.

3.3 Channel $e\gamma \to eH$

There is also literature devoted to this process (see, e.g., [8–10] and references therein).

We attempted a semi-tuned comparison of the total cross sections between Table I of [8, 9] and SANC for the three cms energies $\sqrt{s} = 500$, 1000, 1500 GeV and a wide range for the Higgs mass: 110 GeV $\le M_H \le$ 400 GeV.

Table 1. Comparison for the total width between [14, 15] and SANC in the Born approximation

E_γ, GeV	Γ, GeV, [15]	Γ, GeV, [14]	Γ, GeV, SANC	
70	2.0490(1)	2.0489(1)	2.0491(1)	$\times 10^{-9}$
50	1.4187(1)	1.4189(1)	1.4188(1)	$\times 10^{-8}$
10	1.0029(1)	1.0030(1)	1.0030(1)	$\times 10^{-7}$
1	2.6265(2)	2.6266(1)	2.6264(1)	$\times 10^{-7}$
0.1	4.3329(2)	4.3325(1)	4.3326(1)	$\times 10^{-7}$
0.01	unstable	unstable	6.0474(1)	$\times 10^{-7}$

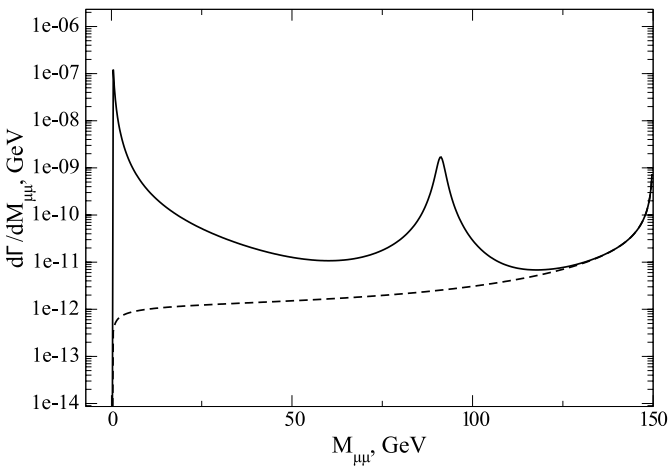

Fig. 6. Invariant mass distribution of the $\mu^+\mu^-$ pair. Both the Born (*dashed*) and one-loop level (*solid line*) results are shown

Table 2. Decay width for variuos cut values of s_q at the Born and one-loop levels

N N	$s_{q\min}$, GeV	$s_{q\max}$ GeV	Γ^{Born}, 10^{-8} GeV	$\Gamma^{\text{Born+1-loop}}$, 10^{-6} GeV
			α scheme	
1	$2m_\mu$	148.997	23.499	1.7536
2	$2m_\mu$	139.642	8.9737	1.6239
3	M_Z-40	M_Z+40	5.5040	1.2443
4	M_Z-20	M_Z+20	2.0188	1.1822
			$G_{\rm F}$ scheme	
1	$2m_\mu$	148.997	24.325	1.8152
2	$2m_\mu$	139.642	9.2891	1.6810
3	M_Z-40	M_Z+40	5.6975	1.2880
4	M_Z-20	M_Z+20	2.0898	1.2238

We tried to use all the masses we managed to find in the paper and the convention of coupling for an "almost on-shell photon". In Table 4 we show the total cross sections σ and the relative difference δ between the two calculations ($\delta = \sigma[8,9]/\sigma[\text{SANC}] - 1$, (%)). As is seen, the difference in the vast majority of points is below 1% and shows an irregular behavior pointing to its numerical origin (our numbers are calculated with REAL*16). Given these observations, we consider the two results to be in very good agreement.

4 Conclusions

This paper is devoted to the description of the implementation of the complete one-loop electroweak calculations for the process $f_1\bar{f}_1 H\gamma \to 0$ into the SANC framework.

We presented analytical expressions for the covariant amplitudes and its form factors, unique for any cross channel and for the helicity amplitudes for each of three cross channel processes: $f_1\bar{f}_1 \to H\gamma$, $H \to f_1\bar{f}_1\gamma$ and $f_1\gamma \to f_1 H$. To be assured of the correctness of our analytical results, we observe the independence of the form factors on the gauge parameters (all calculations were done in R_ξ gauge), the validity of the Ward identity for a covariant amplitude, and finally, the SANC results for these processes were compared with other independent calculations. For the an-

Table 3. SANC, resonance one-loop and complete one-loop approximations

$s_{q\min}$, GeV	$\Gamma^{\text{Res 1-loop}}$, 10^{-6} GeV		$\Gamma^{\text{1-loop}}$ 10^{-6} GeV	
	α	$G_{\rm F}$	α	$G_{\rm F}$
$2m_\mu$	1.17006	1.2112	1.54394	1.59822
1	1.17006	1.2112	1.45652	1.50773
10	1.17006	1.2112	1.29776	1.34339
30	1.16981	1.2109	1.22548	1.26857
50	1.16771	1.2088	1.19604	1.23809
70	1.15659	1.1973	1.17259	1.21381

Table 4. H production channel, SANC and [8, 9]

$M_H/\sqrt{s}$	SANC	500 [8, 9]	δ	SANC	1000 [8, 9]	δ	SANC	1500 [8, 9]	δ
80	8.40	8.38	−0.2	9.31	9.29	−0.2	9.76	9.74	−0.2
100	8.85	8.85	0	9.95	9.94	−0.1	10.48	10.5	−0.2
120	9.77	9.80	0.3	11.16	11.2	0.4	11.80	11.8	0
140	11.76	11.8	0.3	13.68	13.7	0.1	14.52	14.6	0.6
160	20.91	21.1	0.9	24.82	25.0	0.7	26.48	26.6	0.5
180	20.67	20.9	1.1	25.04	25.3	1.0	26.81	27.0	0.7
200	16.99	17.2	1.2	21.05	21.2	0.7	22.64	22.8	0.7
300	5.90	5.97	1.2	8.44	8.53	1.0	9.33	9.43	1.1
400	1.64	1.64	0	2.74	2.78	1.5	3.15	3.18	1.0

nihilation channel, $f_1\bar{f}_1 \to H\gamma$, we found our results for the cross section dependence on the Higgs boson mass to be in a good agreement with [7]. Also, we observe that the cross section depends quite strongly on the top quark mass. Our tree level results for the decay $H \to f_1\bar{f}_1\gamma$ were compared with [14, 15], and we have found agreement better than 10^{-3} (which is within the statistical errors of a Monte Carlo integration). As was expected, the main contribution to the decay width comes from the one-loop corrections, and the major part of this contribution is due to a Z resonance. We have shown that radiative corrections heavily change also the shape of the invariant mass distribution of the $\mu^+\mu^-$ pair. We recognize the importance of the complete one-loop calculation over the one-loop resonance approximation, which even in the presence of the strong cuts on s_q works with percent accuracy. For the channel $f_1\gamma \to f_1 H$, the comparison of the SANC one-loop predictions with the results of [8, 9] has shown very good agreement in a wide range of cms energies and Higgs boson masses.

All processes are implemented at Level 1 of the symbolic FORM [19] calculations and Level 2, where the s2n.f package produces numerical results. One should emphasize however, that the s2n.f codes are not yet accessible from the system, because we had to use a REAL*16 compiler and libraries (both SANC and LoopTools [20]) which are not yet integrated into the system. These codes may be obtained from the authors by request.

Acknowledgements. This work is partly supported by INTAS grant No. 03-51-4007, by the EU grant mTkd-CT-2004-510126 in partnership with the CERN Physics Department and by the Polish Ministry of Scientific Research and Information Technology grant No. 620/E-77/6.PRUE/DIE 188/2005-2008 and by the Russian Foundation for Basic Research grant No. 07-02-00932.

Appendix

In a recent paper [17] we presented an extension of SANC "Processes" tree in the $ffbb$ sector, comprising the version V.1.10. In this paper we realize its further extension by inclusion of the process $f_1\bar{f}_1 HA \to 0$ in three cross channels as was pointed out already in Sect. 2.7 of [11]. For this reason, we do not change the SANC version number; it is still V.1.10.

We have modified the content of the node **2f2b** in the EW part of the "Processes" tree; see Fig. 7. The node 2f2b contains menus for $f_1\bar{f}_1 \to HA$, $H \to f_1\bar{f}_1 A$ and $f_1 A \to f_1 H$, which in turn are branched into the nodes for scalar form factors and helicity amplitudes. Contrary to the pre-

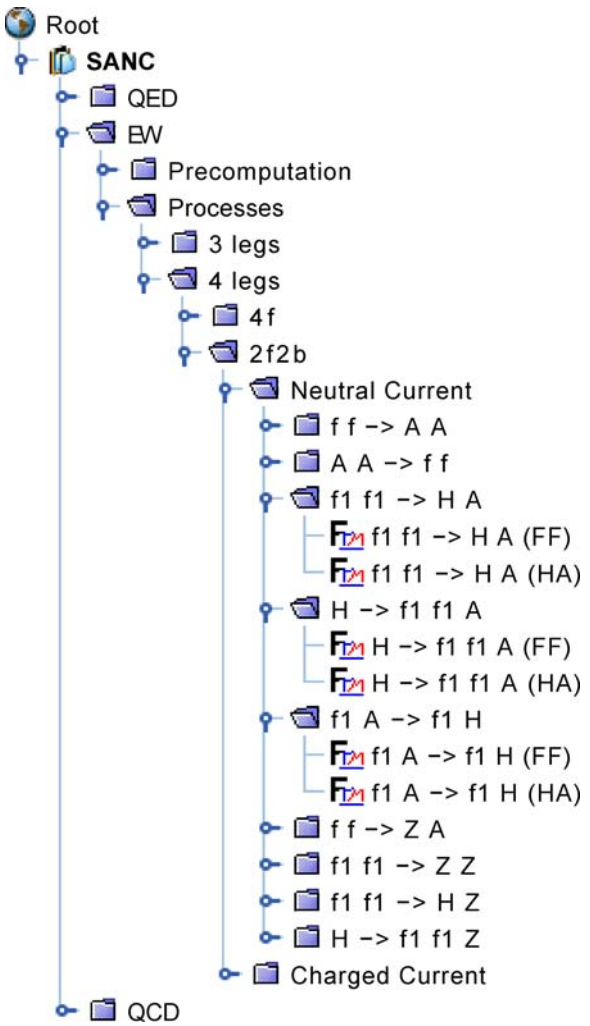

Fig. 7. New processes in the $ffbb$ sector

sentation in Sect. 2.7 of [11], we use now the Born level structure given by (58) of [11]. As a result the FF F_{v1} gets redefined and therefore the HA for the decay channel $H \to f_1\bar{f}_1 A$ become different from those given in (55) of [11] in the parts with F_{v1}. All processes are implemented at Level 1 of the symbolic calculations using FORM3, and Level 2, where the s2n.f package produces numerical results.

References

1. C. Ankenbrandt et al., Phys. Rev. ST Accel. Beams **2**, 081 001 (1999)
2. M. Alsharo'a et al., Phys. Rev. ST Accel. Beams **6**, 081 001 (2003)
3. T. Abe et al., SLAC-R-507 (2001) hep-ex/0106055-58
4. ATLAS Collaboration, CERN-LHCC/99-14 (1999)
5. A. Barroso, J. Pulido, J.C. Romao, Nucl. Phys. B **267**, 509 (1986)
6. A. Abbasabadi, D. Bowser-Chao, D.A. Dicus, W.W. Repko, Phys. Rev. D **52**, 3919 (1995)
7. A. Djouadi, V. Driesen, W. Hollik, J. Rosiek, Nucl. Phys. B **491**, 6 (1997)
8. E. Gabrielli, V.A. Ilyin, B. Mele, Phys. Rev. D **56**, 5945 (1997)
9. E. Gabrielli, V.A. Ilyin, B. Mele, Phys. Rev. D **58**, 119 902 (1998) [Erratum]
10. A.T. Banin, I.F. Ginzburg, I.P. Ivanov, Phys. Rev. D **59**, 115 001 (1999)
11. A. Andonov et al., Comput. Phys. Commun. **174**, 481 (2006)
12. SANC server, Dubna, http://sanc.jinr.ru
13. SANC server, CERN, http://pcphsanc.cern.ch
14. CompHEP Collaboration, E. Boos et al., Nucl. Instrum. Methods A **534**, 250 (2004)
15. F. Yuasa et al., Prog. Theor. Phys. Suppl. **138**, 1 (2000)
16. T. Sjostrand, S. Mrenna, P. Skands, JHEP **0605**, 026 (2006)
17. D. Bardin, S. Bondarenko, L. Kalinovskaya, G. Nanava, L. Rumyantsev, W. von Schlippe, SANCnews: Sector ffbb, hep-ph/0506120
18. G. Passarino, M.J.G. Veltman, Nucl. Phys. B **160**, 151 (1979)
19. J.A.M. Vermaseren, New features of FORM, math-ph/0010025
20. T. Hahn, M. Perez-Victoria, Comput. Phys. Commun. **118**, 153 (1999)